Available online at www.sciencedirect.com
ScienceDirect
Journal of Computational Physics 220 (2006) 88–108
JOURNAL OF COMPUTATIONAL PHYSICS
www.elsevier.com/locate/jcp

Unconditionally positive implicit procedure for two-equation turbulence models: Application to k–ω turbulence models

Y. Moryossef [a,*], Y. Levy [b,1]

[a] *Faculty of Aerospace Engineering, Technion, Israel Institute of Technology, Haifa 32000, Israel*
[b] *Israeli CFD Center, Zikhron Yaakov 30900, Israel*

Received 21 July 2005; received in revised form 10 March 2006; accepted 2 May 2006
Available online 21 June 2006

Abstract

A new general implicit procedure that guarantees the positivity of turbulence model equations dependent variables is presented. The implicit procedure is based on designing the implicit Jacobian to be an M-matrix. A unified approach for the treatment of the convection, diffusion and source terms is introduced and employed. An appropriate design of the M-matrix guarantees the positivity of the turbulence equation dependent variables for any time step, without the use of any clipping. The procedure is employed and demonstrated using a k–ω turbulence model. An efficient construction of the Jacobian matrix is proposed, resulting in diagonal matrices. The model is tested by simulating three test cases of two- and three-dimensional complex flow fields. Results from the numerical simulations show that the new procedure exhibits very good convergence characteristics, is extremely robust, and always preserves the positivity of the turbulence variables.

Keywords: Implicit method; Turbulence model; Positivity preservation; Numerical stiffness; Computations; Source term

1. Introduction

Computational fluid dynamics analysis in research and development as well as in design processes has become a widespread tool. Naturally, realistic turbulent flow simulations solving the Reynolds-averaged Navier–Stokes (RANS) equations are of primary interest. As a result of averaging, RANS equations contain an extra term called the Reynolds stress tensor. Turbulence models that are based on the second-moment closure approach (Reynolds stress models) are regarded as the most advanced models. However, Reynolds stress models tend to be complex and their application requires large computer resources.

* Corresponding author.
E-mail addresses: yairm@bellini.technion.ac.il (Y. Moryossef), yuval@iscfdc.co.il (Y. Levy).
[1] CEO.

0021-9991/$ - see front matter
doi:10.1016/j.jcp.2006.05.001

Two-equation closure models, such as the k–ω or k–ϵ models are probably among the most popular two-equation turbulence models. There are two main issues concerning two-equation models. The first is concerned with the ability of a model to best simulate the flow physics and the main characteristics of the flow. The second issue stems from the actual implementation of the turbulence model in a flow solver and is the objective of the current paper.

Turbulence model equations take the form of a transport equation that consists of convection, diffusion, and source terms. The source term can be strongly nonlinear, containing a different time scale than the convection and diffusion terms, and therefore may become the source of numerical stiffness. The numerical stiffness calls for a special numerical treatment. An inappropriate treatment may result in numerical instability and in a loss of positivity of the turbulence variables. The positivity of the turbulence variables must be kept to guarantee a solid physical basis.

Huang and Coakely [11] conducted turbulent flow simulations using the k–ϵ turbulence model of Launder and Sharma [18] and the original k–ω turbulence model of Wilcox [28]. They designed an unconditionally stable implicit scheme by diagonalizing the convection and diffusion Jacobians. In addition, the source term was implicitly treated only with respect to its negative part. Menter [23] introduced his k–ω shear-stress transport model (SST) that was designed to overcome some of the k–ϵ and k–ω weaknesses. To construct a robust implicit scheme, Menter linearized the negative part of the source term and added the absolute value of the cross-diffusion element to the LHS diagonal. However, he had to use a limiter for the production term to prevent the erroneous, unlimited increase of eddy-viscosity levels.

Mavriplis and Martinelli [22] conducted compressible turbulent flow simulations about airfoils using unstructured grids. They chose different time integration methods for the Navier–Stokes equations and the two-equation turbulence model, combined with a multi-grid accelerator. While the Navier–Stokes equations were advanced in time using a multi-stage Runge–Kutta method, the turbulence model equations were integrated using a point implicit method. Based on stability analysis, they were able to find a restrictive time step that kept the positivity of the turbulence variables.

Liu and Zheng [20] derived a strongly coupled explicit time integration method for solving the Navier–Stokes equations using the k–ω turbulence model by Wilcox [28]. They increased the flow solver robustness by treating the negative part of the source term implicitly. From their numerical simulations, they found that ω reached unrealistic low values, resulting in excessively large values of eddy viscosity. They applied a lower cut-off value that was based on physical reasoning to prevent ω from reaching too low values.

Batten et al. [2] used a splitting strategy to maintain the positivity of the turbulence variables. The convection and diffusion fluxes were split into the 'implicit' and 'correction' parts, where only the 'implicit' part was treated implicitly. The source term was also split, into a positive and a negative part where only the negative part was treated implicitly. They still had to introduce a small parameter into their scheme to prevent the turbulence variables from becoming negative or reaching low values.

Ilinca and Pelletier [12,13] suggested an elegant procedure to preserve the positivity of the turbulence variables. They applied their scheme to the standard k–ϵ model and the k–ω model by Wilcox [28]. The idea behind their scheme is rather simple. Turbulence variables are kept positive by switching them to logarithmic variables, $K = \ln(k)$ and $\Omega = \ln(\omega)$. Ilinca and Pelletier showed that the use of logarithmic variables dictate a smoother variation, leading to an improved flow prediction, resulting in an increase to their flow solver robustness. Yet, since the logarithmic variables are not suitable for homogeneous wall boundary conditions, as given for the turbulent kinetic energy, i.e. $k = 0$, they used a wall function.

Based on the authors experience, application of the idea by Ilinca and Pelletier replaces the problem of a lower bound with a problem of an upper bound. Namely, although the positivity of the turbulence variable is guaranteed, the eddy viscosity can reach unrealistically large values. The problem of an upper bound is also reflected in the work by Luo et al. [21] who adopted the logarithmic variables for a k–ϵ model using a wall function. They had to apply an upper limit to the turbulent viscosity to keep their simulations stable.

Merkle et al. [25] suggested to split the exact Jacobian of the source term based on its eigenvalues. The eigenvalue matrix is split into a positive and a negative part and is subsequently multiplied by the eigenvectors to obtain two matrices. Implicit treatment is applied only to the matrix that resulted from the negative eigenvalues. Merci et al. [24] used the exact Jacobian method proposed by Merkle et al. [25] to derive the implicit

Jacobian of the k–ϵ model by Yang and Shih [31] and of the low-Reynolds k–ω model by Wilcox [29]. However, they still had to apply a lower limit to the turbulence variables to preserve positivity.

Du and Wu [8,9] proposed another strategy, called the mixed analytical–numerical method in which, the high-Reynolds terms of the source term are integrated analytically. Then, the analytical solution is incorporated into the numerical integration, together with the convection, diffusion, and low-Reynolds terms of the source term. They applied their method to various k–ϵ turbulence models. Du and Wu [8] successfully simulated the compressible flow about two airfoils and inside a transonic diffuser. Their simulations show that the method is stable and that it has rapid convergence characteristics. However, their method can not guarantee the positivity of the turbulence variables. Moreover, they had to limit the production part of source term in the turbulence kinetic energy equation.

In the current paper, a general implicit procedure that preserves the positivity of the turbulence variables is proposed. The new procedure is robust, stable, and positivity is kept without the use of any turbulence variables clipping. Moreover, in all simulations considered in the current work, no source term bounding was required. The current paper focuses on the application of the new procedure to the k–ω turbulence model.

2. Governing equations

The Navier–Stokes equations and a typical two-equation turbulence model governing three-dimensional flows may be expressed in Cartesian coordinates and a dimensionless form as follows:

$$\frac{\partial U}{\partial t}+\frac{\partial(F_{\mathrm{c}}-F_{\mathrm{v}})}{\partial x_j}=S \tag{1}$$

The vector U denotes the dependent variables vector:

$$U=\begin{Bmatrix}\rho\\ \rho u_j\\ E\\ \rho\varphi_l\end{Bmatrix} \tag{2}$$

where ρ is the fluid density, $u_j=\{u,v,w\}^{\mathrm{T}}$ are the Cartesian velocity vector components, E is the total energy and $\rho\varphi_l=\rho\{\varphi_1,\varphi_2\}^{\mathrm{T}}$ denotes the dependent variables of the two-equation turbulence model.

The convection flux vector is

$$F_{\mathrm{c}}=\begin{Bmatrix}\rho u_j\\ \rho u_j u_i+p\delta_{ij}\\ \rho u_j H\\ \rho u_j\varphi_l\end{Bmatrix} \tag{3}$$

where p denotes the pressure and H denotes the total enthalpy. The diffusion flux vector is given by

$$F_{\mathrm{v}}=\frac{M_\infty}{Re_\infty}\begin{Bmatrix}0\\ \tau_{ij}\\ \beta_j\\ \mu_{\varphi_l}\frac{\partial\varphi_l}{\partial x_j}\end{Bmatrix} \tag{4}$$

where M_∞ is the free stream Mach number and Re_∞ is the reference Reynolds number. The stress tensor, τ_{ij}, can be written as the sum of the viscous and the Reynolds stress tensors

$$\tau_{ij}=\tau_{ij}^{L}+\tau_{ij}^{T} \tag{5}$$

where the viscous part is

$$\tau_{ij}^{L}=\mu\left[\left(\frac{\partial u_i}{\partial x_j}+\frac{\partial u_j}{\partial x_i}\right)-\frac{2}{3}\delta_{ij}\frac{\partial u_k}{\partial x_k}\right] \tag{6}$$

Based on the Boussinesq assumption, the Reynolds stresses are

$$\tau_{ij}^{T} = \mu_{\mathrm{t}}\left[\left(\frac{\partial u_i}{\partial x_j}+\frac{\partial u_j}{\partial x_i}\right)-\frac{2}{3}\delta_{ij}\frac{\partial u_k}{\partial x_k}\right]-\frac{2}{3}\rho k\delta_{ij}\frac{Re_\infty}{M_\infty} \tag{7}$$

where μ and μ_{t} are the laminar and the turbulent viscosities, respectively, and k represents the turbulence kinetic energy. The terms β_j are defined by

$$\beta_j = u_j\tau_{ij} - q_j \tag{8}$$

The heat conduction terms are given by

$$q_j = -\left(\frac{\mu}{Pr}+\frac{\mu_{\mathrm{t}}}{Pr_{\mathrm{t}}}\right)\frac{\gamma}{\gamma-1}\frac{\partial\left(\frac{p}{\rho}\right)}{\partial x_j} \tag{9}$$

where Pr is the molecular Prandtl number, set as $Pr = 0.72$ and Pr_{t} is the turbulent Prandtl number, set to $Pr_{\mathrm{t}} = 0.9$. The turbulent diffusion flux vector is defined as

$$\mu_{\varphi_l}\frac{\partial\varphi_l}{\partial x_j} = \left\{(\mu+\sigma_{\varphi_1}\mu_{\mathrm{t}})\frac{\partial\varphi_1}{\partial x_j},(\mu+\sigma_{\varphi_2}\mu_{\mathrm{t}})\frac{\partial\varphi_2}{\partial x_j}\right\}^{\mathrm{T}} \tag{10}$$

where σ_{φ_l} is the appropriate Prandtl numbers. In the present work, the source vector, denoted by S, arises only due to the turbulence equations and therefore may be represented by

$$S = \{0,\quad 0,\quad 0,\quad 0,\quad 0,\quad s_l\}^{\mathrm{T}} \tag{11}$$

where $s_l = \{s_1, s_2\}$. The Navier–Stokes equations are closed using the equation of state for a perfect gas

$$p = (\gamma-1)\left[E-\frac{1}{2}\rho(u^2+v^2+w^2)\right] \tag{12}$$

3. Numerical method

3.1. Spatial discretization

The integral form of Eq. (1) can be expressed as follows:

$$\frac{\partial}{\partial t}\int_V U\,\mathrm{d}V + \int_A (F_{\mathrm{c}}-F_{\mathrm{v}})\cdot\vec{n}\;\mathrm{d}A = \int_V S\,\mathrm{d}V \tag{13}$$

where $\vec{n}$ is the outward-pointing unit normal vector to the control volume.

The semi-discretized form for a non-deforming grid is

$$V_i\frac{\mathrm{d}U_i}{\mathrm{d}t} = -\sum_{j\in N(i)}(F_{\mathrm{c},f_{ij}}-F_{\mathrm{v},f_{ij}})A_{f_{ij}} + S_iV_i \tag{14}$$

where U_i is the vector of cell-averaged dependent variables and S_i is the cell source term. The terms $F_{\mathrm{c},f_{ij}}$ and $F_{\mathrm{v},f_{ij}}$ are the convection and diffusion fluxes normal to the interface f_{ij}, respectively. The term V_i is the cell volume and t is the time step. The term $A_{f_{ij}}$ is the face area and $N(i)$ is the set of cell neighbors.

The convection flux vector is computed at the cell interface by using the HLLC scheme as proposed by Batten et al. [2]. For a first order accurate convection flux, the left and right state vectors are taken as the corresponding cell center values. For higher accuracy, information beyond the nearest neighbors is required. In the present study, second order accuracy is achieved by a linear reconstruction using Green's theorem based on the procedure developed by Jawahar and Kamath [15]. The limiter proposed by Venkatakrishnan [27] is used to suppress oscillations in the solution.

The diffusion flux vector is discretized employing the central differencing suggested by Jawahar and Kamath [15] as a part of their effort to construct a uniform procedure for the discretization of the Navier–Stokes equations. The primitive variables and the laminar and turbulent viscosities appearing in the diffusion flux are obtained by simple averaging of the two adjacent cell center values.

3.2. Time integration

The most simple time integration method is the explicit time integration, usually combined with a multigrid accelerator. Explicit schemes are simple to code and to parallelize. However, due to the CFL restriction, the time step is severely limited and the time integration required can be impractical for realistic three-dimensional flows. Alternatively, implicit time integration benefits from higher time steps and better stability and convergence characteristics. Implicit time integration of the Navier–Stokes and the turbulence equations can be conducted in a coupled or in an uncoupled manner. Although coupled integration may result in a more efficient solution in terms of CPU time [1], an uncoupled procedure is easy to implement and it provides enhanced flexibility in designing special treatment for the turbulence model equations. Therefore, the time integration that is adopted herein is the implicit method in an uncoupled manner. Since the present work concerns steady state solutions only the backward Euler-implicit first-order time integration is used.

Using time linearization, Eq. (14) can be rewritten in a general delta form as follows:

$$\left[\frac{V}{\Delta t}I - \frac{\partial R}{\partial U}\right]^n \Delta U^n = R^n \tag{15}$$

where I is the identity matrix and

$$R^n = -\sum \tilde{F}^n A_f + VS^n \tag{16}$$

and $\tilde{F} = F_{c,f_{ij}} - F_{v,f_{ij}}$. The Δ operator is the increment between time level n and $n+1$. Note, the Jacobian $\frac{\partial R}{\partial U}$ is properly derived for an uncoupled method. Eq. (15) is solved using the block lower-upper Gauss–Seidel (BLU-SGS) developed by Chen and Wang [5]. The BLU-SGS scheme is similar to the original LU-SGS approximate factorization scheme developed by Jameson and Yoon [14] with one exception. In contrast to the LU-SGS scheme, in the BLU-SGS scheme the block diagonal exact Jacobians are retained. A local time step is used to accelerate the convergence.

4. Unconditionally positive time integration of the turbulence model equations

For convenience and consistency, the same numerical scheme that is used for the time integration of the Navier–Stokes equations is utilized. The advantage of utilizing the same scheme is further realized when conducting unsteady flow simulations.

For simplicity of notation, the set of the discretized turbulence model equations is extracted from Eq. (15) and it is presented in a similar fashion to Eq. (15), namely,

$$\left[\frac{V}{\Delta t}I - \frac{\partial R^{\mathrm{t}}}{\partial U^{\mathrm{t}}}\right]^n \Delta U^{\mathrm{t}^n} = R^{\mathrm{t}^n} \tag{17}$$

where the vector $U^{\mathrm{t}} = \{\rho\varphi_1, \rho\varphi_2\}^{\mathrm{T}}$ denotes the dependent variables of the turbulence model equations and the vector R^{t} signifies the right hand side (residual) of the discretized turbulence model equations.

The goal of the current work is to design the left hand side of Eq. (17), such that the positivity of the vector $U^{\mathrm{t}^{n+1}}$ is guaranteed for any positive vector U^{t^n} and for any time step $\Delta t > 0$. The approach that is adopted herein is a unified approach. It treats the convection, diffusion, and source terms implicit operators in a similar manner. The following definitions are brought to clarify the construction of an unconditionally positive implicit procedure.

Definition 4.1 (*Unconditional positivity*). Let ΔU^{t^n} be the increment between time levels defined by $\Delta U^{\mathrm{t}^n} \equiv U^{\mathrm{t}^{n+1}} - U^{\mathrm{t}^n}$. A numerical method is unconditionally positive, if $U^{\mathrm{t}^{n+1}} > 0$ for any given $U^{\mathrm{t}^n} > 0$ and for any time step $\Delta t > 0$.

Definition 4.2 (*Nonnegative, positive diagonal* (*NPD*) *matrix*). A matrix $A = (a_{ij} \in R^{n\times n})$ is a nonnegative positive diagonal matrix if $a_{ij} \geqslant 0$ for $j \neq i$ and $a_{ii} > 0$.

Definition 4.3 (*M Matrix*). Consider a matrix $B = (b_{ij} \in R^{n\times n})$ such that $b_{ii} > 0$ and $b_{ij} \leqslant 0$ for $j \neq i$. The matrix B can then be expressed in the form

$$B = sI - C, \quad s > 0, \quad C \geqslant 0, \tag{18}$$

Such a matrix $B = (b_{ij} \in R^{n\times n})$ for which $s \geqslant \rho(C)$, $\rho(C)$ is the spectral radius of the matrix C, is called an M-matrix [3].

Corollary 4.1. *A matrix* $B = (b_{ij} \in R^{n\times n})$ *is an M-matrix iff its entries satisfy the following conditions*

(1) $b_{ii} > 0$
(2) $b_{ij} \leqslant 0$, $j \neq i$
(3) $b_{ii} + \sum_{\substack{j=1 \\ j\neq i}}^{n} b_{ij} > 0$

The last definition is very helpful in designing an M-matrix and from here on any reference to the definition of an M-matrix is with regard to Corollary 4.1.

In the context of the current work, the most important features of an M-matrix are: first, its inverse exists; and second, the inverse is a nonnegative diagonal positive (NPD) matrix [3]. These features are found to be pivotal in the design of an unconditionally positive numerical scheme, as can be seen from the following theorem and its proof.

Theorem 4.1. *Let a general numerical scheme be defined as*

$$M_1 U^{t^{n+1}} = M_2 U^{t^n} \tag{19}$$

where the matrix M_1 *is an M-matrix and the matrix* M_2 *is an* NPD *matrix, independent of the time step. Then the numerical scheme is unconditionally positive.*

Proof 4.1. Since the matrix M_1 is an M-matrix its inverse matrix, M_1^{-1}, exists. Therefore the numerical scheme described in Eq. (19) can be rewritten as

$$U^{t^{n+1}} = M_1^{-1} M_2 U^{t^n} \tag{20}$$

In addition, both matrices M_1^{-1} and M_2 are NPD matrices, independent of the time step. Hence, the matrix $M_1^{-1}M_2$ is also an NPD matrix, for any time step, $\Delta t > 0$. Therefore, for any given positive vector U^{t^n} and any time step, $\Delta t > 0$, the vector $U^{t^{n+1}}$ is also positive. This completes the proof. □

An unconditionally positively scheme can be designed by rewriting Eq. (17) in terms of Theorem 4.1. Inspired by the numerical treatment of Spalart and Allmaras [26] to their one equation turbulence model, the construction of such a scheme is presented below:

Let the residual of the turbulence equations, R^t, be rewritten as

$$R^t = \widehat{R}^t U^t \tag{21}$$

where $\widehat{R}^t$ is the matrix defined by

$$\widehat{R}^t = \frac{1}{2}\begin{bmatrix} \frac{R_1^t}{U_1^t} & \frac{R_1^t}{U_2^t} \\ \frac{R_2^t}{U_1^t} & \frac{R_2^t}{U_2^t} \end{bmatrix} \tag{22}$$

and therefore

$$\frac{\partial R^t}{\partial U^t} = \widehat{R}^t + \frac{\partial \widehat{R}^t}{\partial U^t} U^t \tag{23}$$

Remark 4.1. It should be emphasized that the reformulation of the right hand side vector, as defined in Eq. (21), is employed to derive the implicit operator only and that the right hand side vector remains unchanged.

Further, in terms of Eq. (23), the implicit delta form of the turbulence model equations (Eq. (17)) can be split and rewritten as

$$\underbrace{\left[\frac{V}{\Delta t}I-\left(\widehat{R}^{\mathrm{t}}+\frac{\partial\widehat{R}^{\mathrm{t}}}{\partial U^{\mathrm{t}}}U^{\mathrm{t}}\right)\right]^{n}}_{N_1}U^{\mathrm{t}^{n+1}}=\underbrace{\left[\frac{V}{\Delta t}I-\left(\frac{\partial\widehat{R}^{\mathrm{t}}}{\partial U^{\mathrm{t}}}U^{\mathrm{t}}\right)\right]^{n}}_{N_2}U^{\mathrm{t}^{n}}+\underbrace{(R^{\mathrm{t}^{n}}-\widehat{R}^{\mathrm{t}^{n}}U^{\mathrm{t}^{n}})}_{V_{rl}} \tag{24}$$

To design an unconditionally positive scheme, Eq. (24) should satisfy the following conditions. First, it should be shown that the vector V_{rl} is zero or that is could be brought to the form

$$V_{rl}=N_3U^{\mathrm{t}} \tag{25}$$

where N_3 is an NPD matrix; and second, the matrices N_1 and N_2 should be adjusted to form an M-matrix and an NPD matrix, respectively. Theoretically, the vector V_{rl} is identically zero (see Eq. (21)). Practically, it can be guaranteed only if the spatial discretization on the left hand side is identical to that of the right hand side.

The matrix N_1 is actually the implicit operator of Eq. (17) and the matrix N_2 originates from the same operator. In designing N_1 to be an M-matrix, one should verify that all terms in the matrix $\frac{\widehat{\partial R^{\mathrm{t}}}}{\partial U^{\mathrm{t}}}U^{\mathrm{t}}$ are negative. This guarantees that N_2 is an NPD matrix and that the turbulence model equations have been brought to the Theorem 4.1 form. However, the design of the appropriate N_1 matrix is not straight forward and it requires further modifications. As will be shown, flexibility in designing the scheme is enhanced by splitting the residual vector into its positive and negative parts. Moreover, the construction of the appropriate N_1 matrix is simplified.

Let the right hand side vector, R^{t}, be divided into a positive and a negative part as follows:

$$\begin{aligned}R^{\mathrm{t}}&=R^{\mathrm{t}}_p-R^{\mathrm{t}}_n\\ R^{\mathrm{t}}_p&=\frac{1}{2}(|R^{\mathrm{t}}|+R^{\mathrm{t}})\\ R^{\mathrm{t}}_n&=\frac{1}{2}(|R^{\mathrm{t}}|-R^{\mathrm{t}})\end{aligned} \tag{26}$$

then the matrix N_1 may be rewritten as

$$N_1=\frac{V}{\Delta t}I+\left(\widehat{R}^{\mathrm{t}}_n-\widehat{R}^{\mathrm{t}}_p\right)+\left(\frac{\partial\widehat{R}^{\mathrm{t}}_n}{\partial U^{\mathrm{t}}}U^{\mathrm{t}}-\frac{\partial\widehat{R}^{\mathrm{t}}_p}{\partial U^{\mathrm{t}}}U^{\mathrm{t}}\right) \tag{27}$$

The treatment of the diagonal entries, namely N_{1ii}, is separated from the treatment of the off diagonal entries, N_{1ij}. Three different strategies can be followed to appropriately modify the diagonal entries of the N_1 matrix.

4.1. Strategy 1–1

Consider all the diagonal elements such that only positive contributions are added as follows:

$$N_{1ii}-\frac{V}{\Delta t}I=\widehat{R}^{\mathrm{t}}_n+\underbrace{\mathrm{Max}\left[-\widehat{R}^{\mathrm{t}}_p,0\right]}_{\text{identically zero}}+\mathrm{Max}\left[\frac{\partial\widehat{R}^{\mathrm{t}}_n}{\partial U^{\mathrm{t}}}U^{\mathrm{t}},0\right]+\mathrm{Max}\left[-\frac{\partial\widehat{R}^{\mathrm{t}}_p}{\partial U^{\mathrm{t}}}U^{\mathrm{t}},0\right] \tag{28}$$

4.2. Strategy 1–2

The diagonal entries $-\widehat{R}^{\mathrm{t}}_p$ and $-\frac{\partial\widehat{R}^{\mathrm{t}}_p}{\partial U^{\mathrm{t}}}U^{\mathrm{t}}$ are neglected, resulting in

$$N_{1ii}-\frac{V}{\Delta t}I=\widehat{R}^{\mathrm{t}}_n+\mathrm{Max}\left[\frac{\partial\widehat{R}^{\mathrm{t}}_n}{\partial U^{\mathrm{t}}}U^{\mathrm{t}},0\right] \tag{29}$$

4.3. Strategy 1–3

Consider all the diagonal entries as follows:

$$N_{1ii} - \frac{V}{\Delta t} I = \mathrm{Max}\left[\widehat{R}^{\mathrm{t}}_n - \widehat{R}^{\mathrm{t}}_p, 0\right] + \mathrm{Max}\left[\frac{\partial \widehat{R}^{\mathrm{t}}_n}{\partial U^{\mathrm{t}}} U^{\mathrm{t}} - \frac{\partial \widehat{R}^{\mathrm{t}}_p}{\partial U^{\mathrm{t}}} U^{\mathrm{t}}, 0\right] \tag{30}$$

There are two simple options to build the off diagonal entries of the matrix N_1.

4.4. Strategy 2–1

$$N_{1ij} = -\widehat{R}^{\mathrm{t}}_p, \quad j \neq i \tag{31}$$

4.5. Strategy 2–2

$$N_{1ij} = \mathrm{Min}[\widehat{R}^{\mathrm{t}}_n - \widehat{R}^{\mathrm{t}}_p, 0], \quad j \neq i \tag{32}$$

The above described strategies guarantee only the first two conditions of Corollary 4.1. It can be shown that the third condition may be enforced if one adopts strategy 1–1 for the diagonal entries combined with strategy 2–2 for the off diagonal entries. Note, adopting strategies 1–1 and 2–2 results in a modification of $\widehat{R}^{\mathrm{t}}$. Therefore, the vector V_{rl} in Eq. (24) is no longer guaranteed to be zero. However, it can be shown that it satisfies Eq. (25) and therefore it does comply with Theorem 4.1.

The above strategies show how to construct an M-matrix from the matrix $N_1 - \frac{V}{\Delta t} I$. Based on Corollary 4.1 it is clear that the matrix N_1 is an M-matrix for any time step, $\Delta t > 0$. This section describes a general approach to design an unconditionally positive scheme for a typical two-equation turbulence model. From here on the paper focuses on k–ω turbulence models.

5. Efficient treatment of the implicit Jacobian of the k–ω turbulence model equations

To simplify the construction of all the block matrices, an efficient procedure is introduced. The idea is to write each of the two turbulence equations as if they were two uncoupled equations. Such a procedure results in block matrices that are all diagonal matrices. The savings in terms of memory storage and CPU time are obvious. As already noted in Remark 4.1, the reformulation of the right hand side vector that is presented below is for the purpose of construction of the left hand side operator only. For simplicity, the idea is presented for a typical high Reynolds k–ω turbulence model:

(1) Substitute the ω terms that appear in the turbulence kinetic energy equation using the explicit expression of μ_{t}, *i.e.*, $\omega = \frac{\rho k}{\mu_{\mathrm{t}}}$.
(2) Substitute the k terms that appear in the specific dissipation rate equation using the explicit expression of μ_{t}, *i.e.*, $k = \frac{\omega \mu_{\mathrm{t}}}{\rho}$.
(3) Substitute the turbulence viscosity term, μ_{t}, that appeared in the original equations (prior to the application of steps 1 and 2), with $\frac{\rho k}{\omega}$.
(4) Derive the implicit operator according to the procedure described in the previous section.

As mentioned above, one may interpret the procedure as an attempt to form two uncoupled equations for each of the dependent variables by substitution. As a results, for the purpose of generating the left hand side operator, the residual vector may be expressed in the form (bearing in mind Remark 4.1):

$$R^{\mathrm{t}} = \left\{ \begin{array}{l} R^{\mathrm{t}}_1[\rho k, (\rho\omega)^n, \mu^n_{\mathrm{t}}] \\ R^{\mathrm{t}}_2[(\rho k)^n, \rho\omega, \mu^n_{\mathrm{t}}] \end{array} \right\} \tag{33}$$

Since R_1^t is now a function of ρk only, and since R_2^t is a function of $\rho\omega$ only, it is justified to further simplify the matrix $\widehat{R}^t$ (Eq. (22)) to take the form:

$$\widehat{R}^t = \begin{bmatrix} \frac{(R_1)_n^t}{\rho k} - \frac{(R_1)_p^t}{\rho k} & 0 \\ 0 & \frac{(R_2)_n^t}{\rho\omega} - \frac{(R_2)_p^t}{\rho\omega} \end{bmatrix} \tag{34}$$

and the Jacobian matrix $\frac{\partial \widehat{R}^t}{\partial U^t} U^t$ becomes

$$\frac{\partial \widehat{R}^t}{\partial U^t} U^t = \begin{bmatrix} \frac{\partial}{\partial(\rho k)}\left(\frac{(R_1)_n^t}{\rho k} - \frac{(R_1)_p^t}{\rho k}\right)\rho k & 0 \\ 0 & \frac{\partial}{\partial(\rho\omega)}\left(\frac{(R_2)_n^t}{\rho\omega} - \frac{(R_2)_p^t}{\rho\omega}\right)\rho\omega \end{bmatrix} \tag{35}$$

where $(R_l)_n^t$ and $(R_l)_p^t$ are as defined in Eq. (26). Note, as mentioned above, both Jacobian matrices are indeed diagonal.

In general, the source terms are treated as a volumetric source (also adopted in the current work). Therefore, off diagonal entries in the matrix N_1 arise only from the convection and diffusion terms. Consequently, the only implicit operator that fulfills the three conditions of an M-matrix (see Corollary 4.1) for the convection and diffusion terms is derived by adopting strategy 1–1 for the diagonal entries combined with strategy 2–2 for the off diagonal entries. The evaluation of the implicit operator of the source term can be conducted by using one of the three strategies 1–1, 1–2, or 1–3. Based on numerical experiments it is found that the implicit source operator that is designed according to strategy 1–3 exhibits the best convergence rate. Therefore, strategy 1–3 is chosen in the current work. In addition, based on the discussion concerning Eq. (24), the convection term of the turbulence model equations is discretized using a first order operator.

6. The k–ω–TNT turbulence model

In the present work, the proposed procedure is applied to the k–ω turbulence model that was proposed by Kok [16], also known as the TNT model. The model takes the form as described in Eqs. (1)–(11) where φ_1 denotes the turbulence kinetic energy, namely $\varphi_1 = k$ and φ_2 denotes the turbulence specific dissipation rate, namely $\varphi_2 = \omega$. The source vector, S^t, takes the general form:

$$S^t = \begin{Bmatrix} P_k - \beta^* \rho k \omega \frac{Re_\infty}{M_\infty} \\ \alpha \frac{\omega}{k} P_k - \beta \rho \omega^2 \frac{Re_\infty}{M_\infty} + C_D \end{Bmatrix} \tag{36}$$

The production term, P_k, is given by

$$P_k = \tau_{ij}^T \frac{\partial u_i}{\partial x_j} \frac{M_\infty}{Re_\infty} \tag{37}$$

The Prandtl numbers are $\sigma_\omega = 0.5$ and $\sigma_k = \frac{2}{3}$. The remaining model constants are $\beta = 0.075$, $\beta^* = 0.09$, $\alpha = \frac{\beta}{\beta^*} - \frac{\sigma_\omega \kappa^2}{\sqrt{\beta^*}}$, with $\kappa = 0.41$. The source term C_D is given as

$$C_D = \sigma_d \frac{\rho}{\omega} \mathrm{Max}\left[\frac{\partial k}{\partial x_j}\frac{\partial \omega}{\partial x_j}, 0\right] \frac{M_\infty}{Re_\infty} \tag{38}$$

where $\sigma_d = 0.5$ and the turbulent viscosity is defined as

$$\mu_t = \rho k/\omega \tag{39}$$

Details of the application of the procedure to the model may be found in Appendix A.

7. Results and discussion

Three well known test cases are simulated and examined using the new implicit procedure. The aim of the tests is twofold: first to verify that the proposed procedure indeed preserves positivity of the turbulence variables, for various cases; and second, to study the convergence characteristics of the new procedure.

The first test case is the separated flow about a NACA 4412 airfoil at high incidence. The second test is the transonic flow about the RAE2822 airfoil. The third test is the high incidence flow about a tangent-ogive cylinder. Although the flow prediction accuracy of the turbulence model is not the main focus of the current work, two different sets of grids were employed for each of the two-dimensional test cases with various CFL numbers examining grid convergence using the proposed procedure. Two CFL numbers and one grid was employed for the three-dimensional case.

In this section, the k–ω turbulence model is denoted as TNT and any reference to the Navier–Stokes equations is denoted by NS. It is important to reemphasize that in all conducted simulations, there was no use of any kind of clipping to the turbulence variables. Nor was there any use of any kind of bounding to any terms of the turbulence model equations.

7.1. Boundary conditions

The boundary conditions considered in this work are set as follows. The inflow turbulent kinetic energy is evaluated according to the relation $k = \frac{3}{2}(\mathrm{Tu} \cdot M_\infty)^2$ where Tu is the turbulence intensity. The inflow turbulence specific dissipation rate is set so that the normalized inflow turbulence viscosity is equal to $\mu_{t_\infty} = 0.1$. At the outflow boundary, the turbulence variables are extrapolated from the interior. The wall boundary condition for the turbulent kinetic energy is set to $k = 0$, while the turbulent dissipation rate at the wall is determined according to Menter [23], and is set to $\omega = 10\frac{6\mu}{\rho\beta(\Delta z_1)^2}\left(\frac{M_\infty}{Re_\infty}\right)^2$, where Δz_1 is the distance of the first cell center, neighboring the wall, from the wall.

7.2. NACA 4412 airfoil

The NACA 4412 test is a well known test for high lift separated flows. In the current work a single incidence of $\alpha = 13.87°$ at a Reynolds number of $Re_\infty = 1.52 \times 10^6$ is examined and compared to the experimental results of Coles and Wadcock [6]. At this incidence, a steady trailing-edge separation is present. Two C-type grids were employed as described in Table 1.

For each of the two grids, the simulations were conducted for 5000 steps using three CFL numbers: 25.0, 50.0 and 100.0. Although the experiments are known to involve a transitional boundary layer, it is not modeled in the current work.

Fig. 1 shows a comparison of the calculated stream-wise velocity profile with the experimental data at six stations along the upper airfoil surface (η is the axis perpendicular to the airfoil surface, see a schematic description in Fig. 2). The calculated results that are presented in the figure are obtained using the fine grid (there were only marginal differences from the results obtained with the coarse grid). The prediction obtained using the TNT model is in good agreement with the experimental results.

The convergence of the turbulence model equations and the Navier–Stokes equations is presented in Fig. 3. The TNT model exhibits excellent convergence for the CFL numbers of CFL = 25.0 and CFL = 50.0, for all the grids that were considered. Also noteworthy is the fact that the convergence characteristics of the turbulence equations and of the Navier–Stokes equations are similar. Consequently, it is recognized that the stability and convergence of the turbulence equations and of the Navier–Stokes equations are in some sense

Table 1
Computational grids for the NACA 4412 airfoil

Grid	Size	Δz_1
Coarse	241×65	1×10^{-5}
Fine	345×101	2×10^{-6}

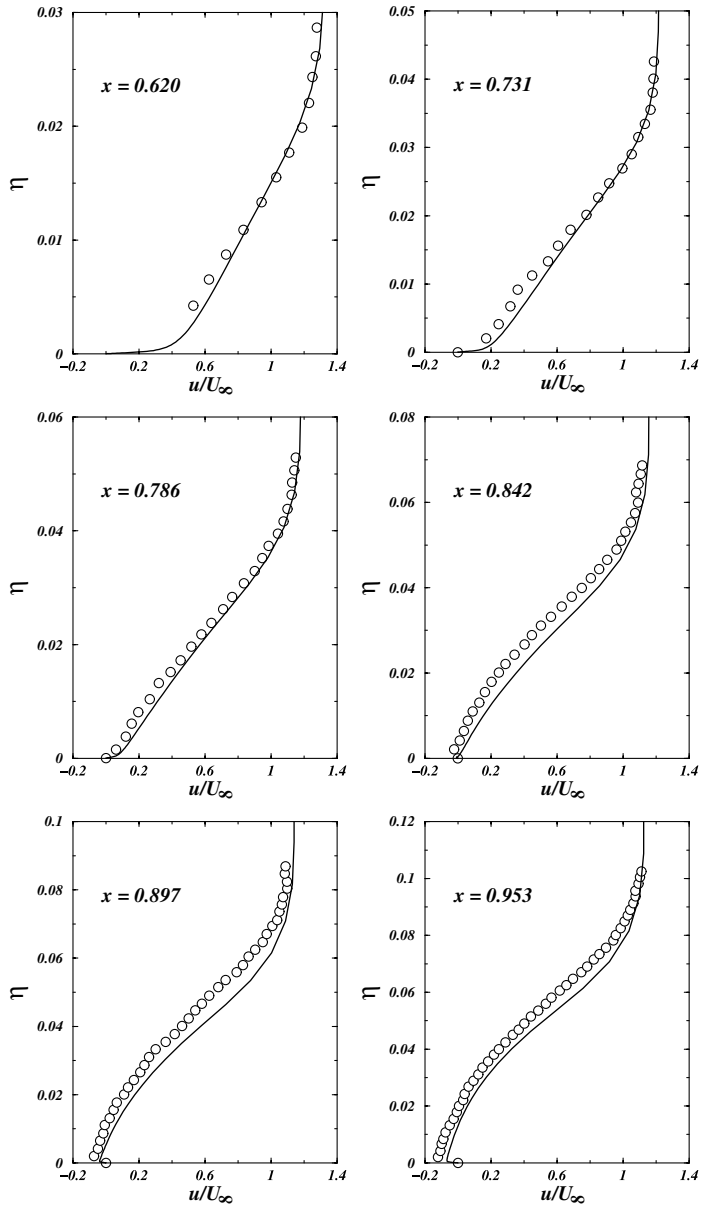

Fig. 1. Comparison between calculated and measured stream-wise velocity profiles at six stations for the NACA 4412 airfoil: ○, experiments [6]; —, TNT model.

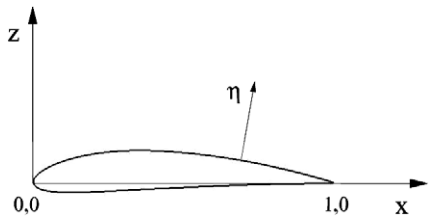

Fig. 2. Schematic description of coordinate axes for the NACA 4412 airfoil.

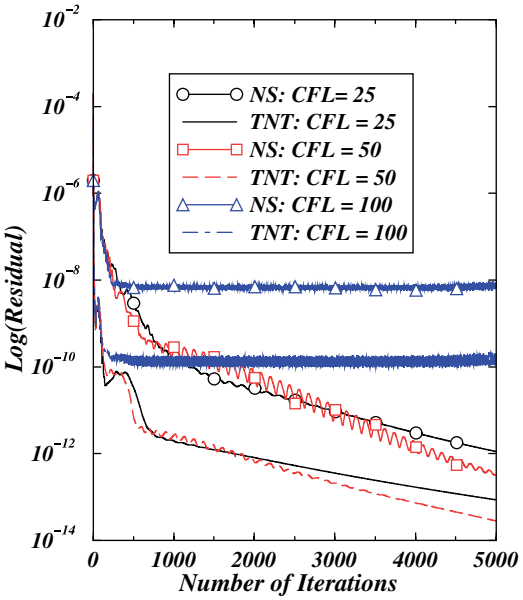

Fig. 3. Convergence behavior of the Navier–Stokes and k–ω equations; NACA 4412 airfoil.

coupled. This can be realized from the fact that the turbulence equations are integrated using the same implicit scheme that is used for the Navier–Stokes equations. Yet, one should note that the source term influence is not included in the stability analyses. The similar convergence characteristics are in accordance with the findings presented by Merci et al. [24]. Namely, although a restriction on the time step due to the source term is required to keep a stable simulation, in practice, the time step limitation derived from the convection and diffusion terms is more restrictive.

To demonstrate the positivity of the turbulence variables, a plot of the minimum turbulent kinetic energy and the minimum turbulence specific dissipation rate history is presented in Fig. 4. The results that are

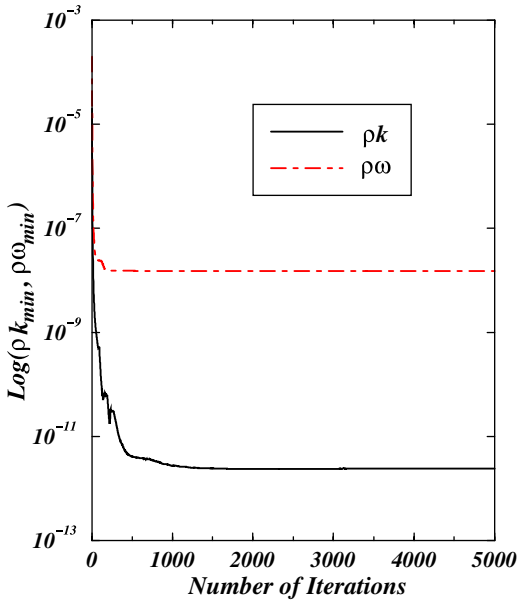

Fig. 4. Minimum k–ω turbulence model dependent variables time history; NACA 4412 airfoil.

presented in the figure were obtained using the coarse grid and a CFL number of CFL = 100.0. No negative values of k or ω, nor extremely low values of k or ω appeared throughout the duration of the numerical simulations. Moreover, the variation of k and ω is quite monotonic and both variables reach their steady state value within 1000 and 250 iterations, respectively. Note that these results are taken from the least stable case, using the highest CFL number, yet the minimum values of the turbulence variables exhibit a monotonic, non-negative behavior.

7.3. RAE2822 airfoil

The RAE2822 supercritical airfoil is another well know test case. It is used for the validation of flow solvers with respect to transonic turbulent flows. The experiment by Cook et al. [7] covers a wide variety of flow conditions. The flow conditions that are used in the current work (their test case number 10) are: a Mach number of $M_\infty = 0.75$, a Reynolds number of $Re_\infty = 6.5 \times 10^6$, and an incidence angle of $\alpha = 3.19°$. In the experiments, transition has been tripped on both the upper and lower surfaces, near the leading edge. Various wind tunnel corrections have been suggested in previous studies. In the present study, the corrections used in the EUROVAL project [10] are adopted. These corrections correspond to the following flow conditions: a Mach number of $M_\infty = 0.754$, a Reynolds number of $Re_\infty = 6.2 \times 10^6$, and an incidence angle of $\alpha = 2.57°$.

Test case number 10 represents a challenging test case for a compressible flow solver. It exhibits a very strong shock which induces boundary layer separation. Note that in the present simulation, the transition was not modeled. Two C-type grids were employed in the current test as given in Table 2.

Numerical simulations were conducted for both grids and two CFL numbers, CFL = 5.0 and CFL = 10.0, for 5000 steps. Fig. 5 contains a comparison of the calculated surface pressure coefficient with that of the experiment [7]. The TNT model predicted the location of the shock downstream compared to the shock location that was experimentally observed. In addition, the pressure recovery after the shock is under predicted. These deficiencies are also found in the work by Catalano and Amato [4] using several k–ω and k–ϵ models, and in the work of Lien and Kalitzin [19] using the $v^2 - f$ four equations turbulence model. Moreover, in all of

Table 2
Computational grids for the RAE2822 airfoil

Grid	Size	Δz_1
Coarse	281×71	1×10^{-5}
Fine	343×95	5×10^{-6}

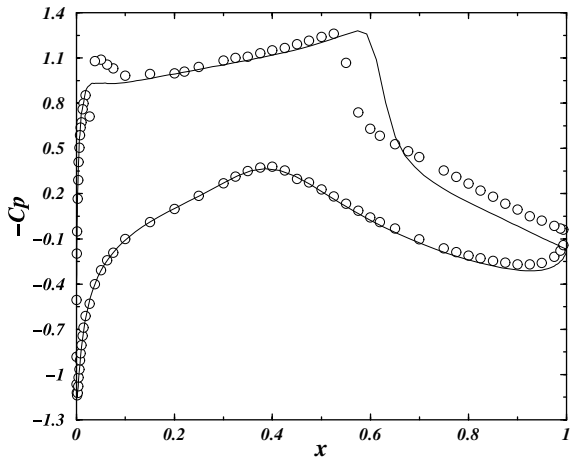

Fig. 5. Comparison between calculations and measured surface pressure coefficient distribution of RAE2822 airfoil: ○, experiments [7]; —, TNT model.

the simulations, the leading edge peak is not captured, most likely due to the fact that the transition was not modeled.

Fig. 6 presents a comparison of the calculated stream-wise velocity with the experimental data at three stations along the upper airfoil surface (η is the axis perpendicular to the airfoil surface). At $x = 0.404$ the flow is attached and the TNT model prediction is in excellent agreement with the experimental results. In contrast, the model fails to accurately predict the velocity profile at the stations $x = 0.65$ and $x = 0.9$, stations that are located downstream of the shock.

A plot of the convergence history that was obtained using the coarse grid is presented in Fig. 7. One can see that the observation made about the convergence characteristics of the NACA 4412 case, holds for the RAE2822 case as well. Moreover, compared to the Navier–Stokes equations, the convergence of the turbulence model equations is even smoother. Specifically, the plot of the convergence history of the turbulence

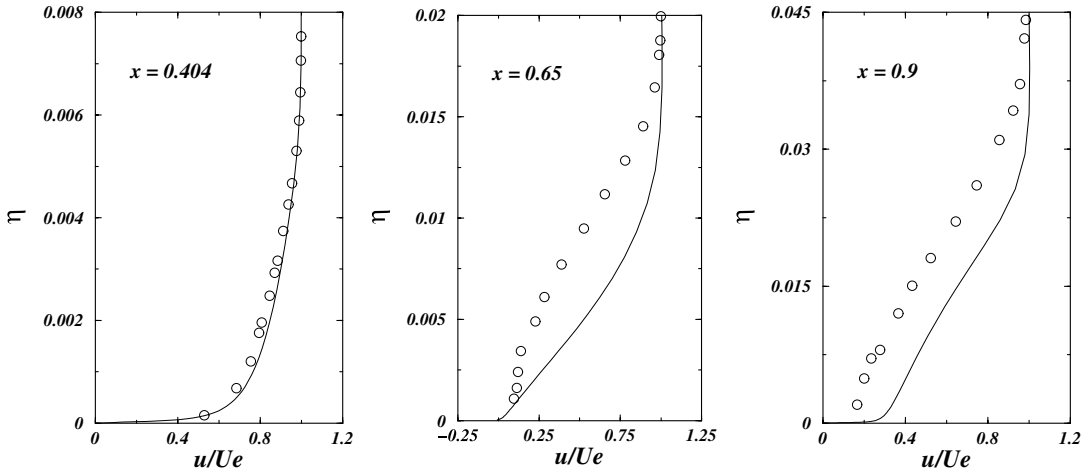

Fig. 6. Comparison between calculated and measured stream-wise velocity profile for the RAE2822 airfoil: ○, experiments [7]; —, TNT model.

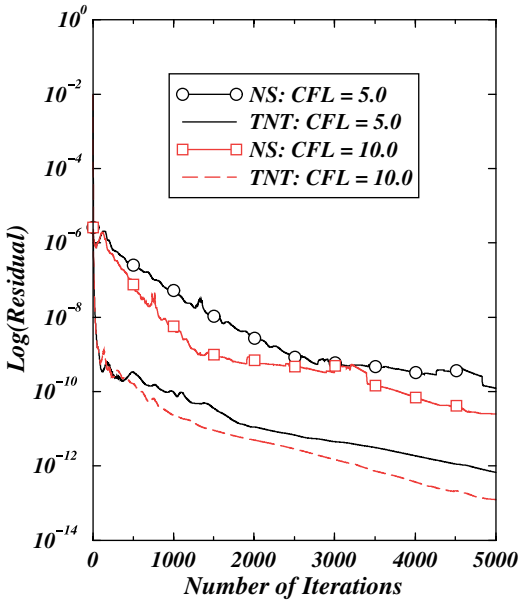

Fig. 7. Navier–Stokes and k–ω equations convergence behavior; RAE2822 airfoil.

model equations lacks the spikes that are present in the Navier–Stokes equations convergence history plot. In addition, the TNT exhibits excellent convergence behavior. The above described behavior is also common to the results obtained using the fine grid.

7.4. Tangent-ogive cylinder

The flow about a tangent-ogive cylinder at high incidence has been extensively studied in the past, both numerically and experimentally. One of the most comprehensive experiments concerning the flow about ogive cylinders was conducted by Lamont in the NASA Ames 12-ft pressure wind tunnel [17]. The geometry of the tangent-ogive cylinder was comprised of a 3.5 caliber ogive and a 4 diameter after-body. Detailed surface-pressure distributions were obtained at Reynolds numbers ranging from $Re_D = 2.0 \times 10^5$ to $Re_D = 4.0 \times 10^6$ and angles of attack ranging from $\alpha = 20°$ to $\alpha = 90°$.

Out of the wide range of flow conditions, the test case that was used for the current work is that of the flow at a Mach number of $M_\infty = 0.2$, an incidence angle of $\alpha = 20°$, and a Reynolds number of $Re_\infty = 4 \times 10^6$. The computed body length was extended 3.0 diameters beyond the physical length of the body, to a total of 10.5 diameters, in order to minimize the effect of the outflow boundary conditions. A single grid having the dimensions $65 \times 72 \times 75$ was generated. The computational mesh extended to 14 body diameters and the first grid point neighboring the wall was placed at 1×10^{-5} diameter from the body.

Based on the experimental results and the wide knowledge concerning the flow at the relatively small incidence angles, the flow field was assumed to be symmetric and therefore, the computational mesh was built accordingly.

The tangent-ogive cylinder test case was chosen to demonstrate that the newly proposed procedure works for complex separated three-dimensional flows as well. The simulations were conducted for two CFL numbers, CFL = 20.0 and CFL = 40.0. Fig. 8 shows a comparison of the calculated circumferential surface pressure coefficient at two longitudinal stations with the experimental results (the origin of the coordinate system is placed at the tip with the x coordinate coinciding with the body symmetry axis and pointing backwards). The comparisons show good agreement of the calculated results with the experimental data.

The convergence history for both CFL numbers is presented in Fig. 9. The convergence plots show excellent convergence for both CFL numbers with similar convergence characteristics. The flow converges to its steady state solution within 1500 steps only, which is quite a low number for the complex flow in question. It is again shown that the convergence behavior of the Navier–Stokes equations and the turbulence model equations is also similar. Throughout the duration of all simulations in this case, no occurrences of negative nor extremely small values of the turbulence variables were observed.

7.5. Effect of perturbed solution on positivity and convergence

To further examine the robustness of the newly proposed procedure, the following numerical experiment was conducted using the RAE2822 airfoil test case with the coarse grid. First, the solution was run for 1000 steps using a CFL number of 10.0. At this point, the residual of the Navier–Stokes equations dropped

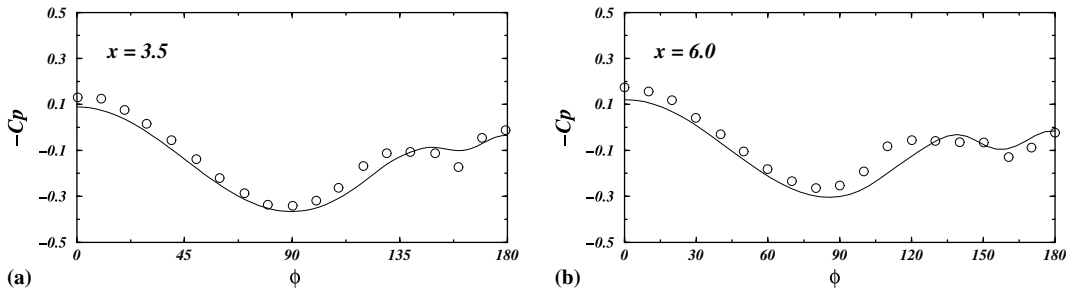

Fig. 8. A comparison of the circumferential surface pressure coefficient at two longitudinal stations: (a) $x = 3.5$, (b) $x = 6.0$: ○, experiments [17]; —, TNT model.

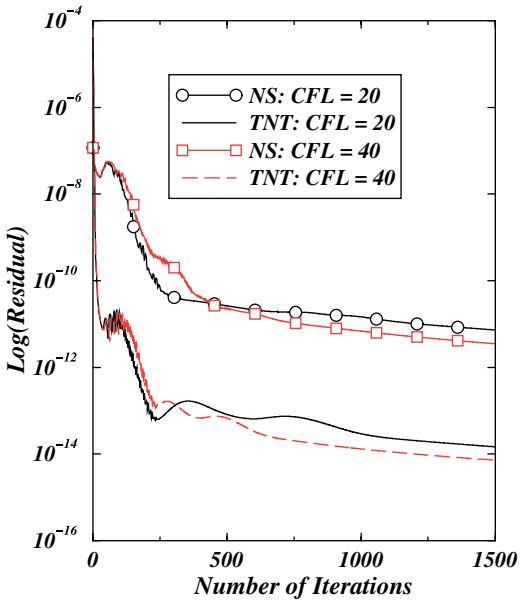

Fig. 9. Navier–Stokes and k–ω equations convergence behavior; Tangent ogive-cylinder.

two orders of magnitude and the residual of the turbulence model equations dropped four orders of magnitude. However, the solution was not fully converged yet. Next, a disturbance was placed in a region defined by $0.4 < x < 0.9$ and $z_u < z < 0.3$ where z_u is the upper airfoil surface (See schematic description in Fig. 10). The domain was chosen to include the shock were the solution is known to exhibit its largest variations. The nature of the disturbance was such that the value of the turbulent kinetic energy was arbitrarily set to a certain extremely low value, k_d. Then, the solution was restarted from that point using the same CFL number (CFL = 10.0) and the values of both the turbulent kinetic energy and the turbulence specific dissipation rate were closely followed. Three simulations, using three values of k_d, namely, $k_d = 1. \times 10^{-20}$, $k_d = 1. \times 10^{-30}$, and $k_d = 1. \times 10^{-40}$ were conducted.

For all three simulations, the turbulence specific dissipation rate showed no noticeable changes (not shown here). The turbulent kinetic energy gradually recovered to higher values and eventually the solution returned to its original convergence course. Fig. 11 shows the history of the minimum turbulent kinetic energy in the flow field. All three plots show an initial drop in the minimum turbulent kinetic energy. The location of the minima was found to always reside very close to the airfoil surface. This behavior can be explained by the fact that the destruction is dominant near the wall. Following the initial drop, the minimum values of turbulence kinetic energy started to rise toward their converged value. This rise is due to the fact that the convection and diffusion terms gradually started to affect the solution. The most important fact arising from this numerical experiment is that the turbulence variables remained positive at all times with a fast recovery. Moreover,

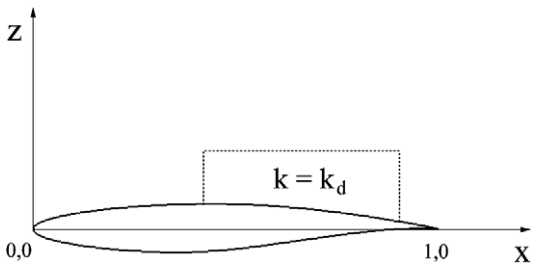

Fig. 10. Schematic description of the region of disturbance in the RAE2822 airfoil flow field.

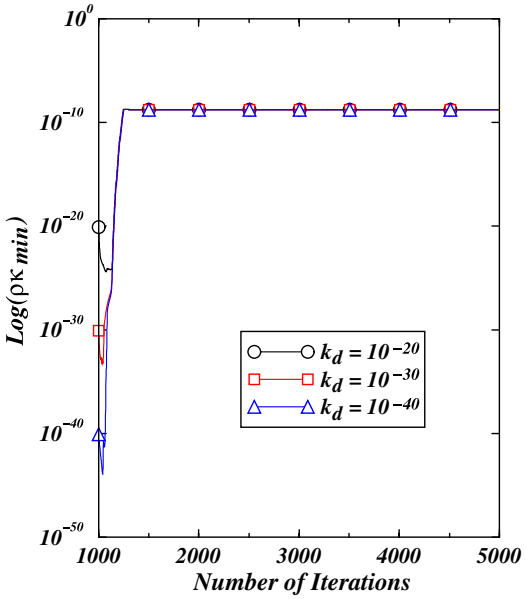

Fig. 11. Time history of minimum turbulent kinetic energy.

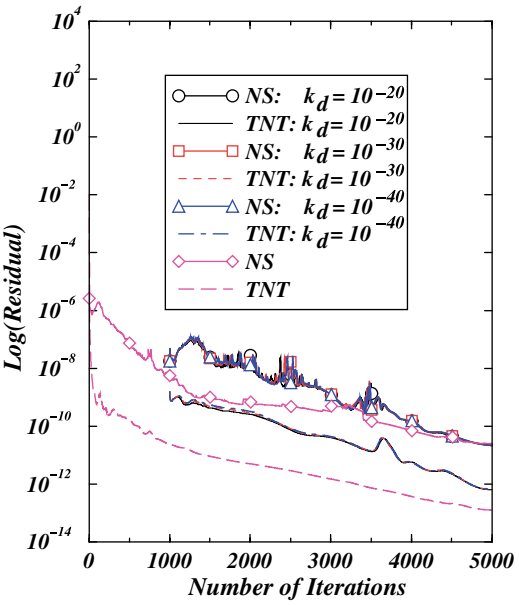

Fig. 12. Convergence history following artificial disturbance.

despite the large numerical disturbance, the convergence characteristic remained the same, and after the recovery of the turbulent kinetic energy values, the whole solution returned to its normal convergence course (see Fig. 12).

8. Concluding remarks

A new unconditionally positive implicit procedure for two-equation turbulence models is developed and presented. The new procedure is validated by applying it to the k–ω–TNT [16] turbulence model. The positiv-

ity of the turbulence variables is analyzed and proved. The scheme robustness and stability are demonstrated using two- and three-dimensional complex flows.

The consistent performance of the implicit procedure is evident from the numerical simulations results. The robustness of the procedure is demonstrated by conducting a special numerical experiment in which a significant disturbance is introduced into the flow field. The numerical experiment shows that for any positive value of the turbulent kinetic energy, even an artificially, extremely low value, positivity is retained. Thus, it is shown that the new scheme follows unconditional positivity as defined in Definition 4.1.

The implicit procedure is characterized by very good convergence rates. Moreover, the convergence behavior of the turbulence equations is similar to that of the Navier–Stokes equations. This is because both are time integrated using the same implicit scheme. The similar convergence shows that the new procedure does not hinder the convergence of the flow solver.

The flexibility in the implementation of the new procedure results in another clear advantage. The implicit procedure can be applied in conjunction with other implicit schemes that are used to solve the Navier–Stokes equations. Further, the procedure can be easily applied to various k–ω turbulence models. Particularly, the procedure was successfully applied to the k–ω–SST model by Menter [23], and to the low and high Reynolds number turbulence models by Wilcox [29,30] and the results exhibited similar behavior to the k–ω–TNT model.

The excellent convergence characteristics are further realized in the context of unsteady flow simulations, especially when the two sets of equations are solved in an uncoupled manner. The extension of the implicit procedure to higher temporal accuracy is straight forward. Using the concept of dual-time stepping it can be proven that an unconditionally positive scheme may be derived for any physical and artificial time steps. Preliminary results of the extended procedure employed to simulate unsteady flow using the concept of dual-time stepping demonstrated the positivity of the turbulence variables.

Acknowledgments

The authors thank Mr. Pietro Catalano for kindly providing his numerical data for comparisons, special thanks are due to Dr. P. Jawahar for his assistance with the implementation of his scheme, and Prof J.B. Greenberg for his valuable comments.

Appendix A

A practical implementation of the new procedure is given hereby for the k–ω–TNT turbulence model [16]. Note, throughout the practical implementation, it is essential to bear in mind Remark 4.1.

The details of the procedure implementation concerning the convection and diffusion fluxes are given for a one-dimensional flow in Cartesian coordinates. Only the turbulence kinetic energy flux terms are considered. The implementation for the turbulence specific dissipation rate is similar. First, the treatment of the implicit diffusion part is addressed. The diffusion flux term of a typical cell i at the interface f_{ij} is given as

$$F_{\mathrm{v},f_{ij}} = \frac{M_\infty}{Re_\infty}\left[(\mu + \sigma_k \mu_\mathrm{t})\frac{\partial k}{\partial x}\right] \tag{A.1}$$

As already mentioned in the paper, the values of the laminar and turbulent viscosities at the interface f_{ij} are calculated by averaging the two corresponding cell values, namely, cell i and its neighbor cell j. In addition, the interface gradient is evaluated using central differencing. Therefore, the diffusion flux is evaluated as:

$$F_{\mathrm{v},f_{ij}} = \frac{M_\infty}{Re_\infty}\frac{1}{2}\left[\left(\mu_i + \mu_j\right) + \sigma_k\left(\mu_{\mathrm{t}i} + \mu_{\mathrm{t}j}\right)\right]\frac{k_j - k_i}{x_j - x_i} \tag{A.2}$$

Step 1 states that ω should be substituted with $\frac{\rho k}{\mu_\mathrm{t}}$ wherever it appears in the turbulence kinetic energy equation. Since ω does not appear in the diffusion flux, step 1 is skipped. Next, step 3 is employed and the diffusion flux is given as:

$$F_{\mathrm{v},f_{ij}} = \frac{M_\infty}{Re_\infty}\frac{1}{2}\left\{(\mu_i+\mu_j)+\sigma_k\left[\left(\frac{\rho k}{\omega}\right)_i+\left(\frac{\rho k}{\omega}\right)_j\right]\right\}\frac{k_j-k_i}{x_j-x_i} \tag{A.3}$$

Next, the first part of the diffusion Jacobian matrix, (see Eq. (23)) namely, $\widehat{F}_{\mathrm{v}}$ is derived. One should distinguish between the treatment of the diagonal and the off diagonal of the Jacobian $\widehat{F}_{\mathrm{v}}$. The diagonal part, $(\widehat{F}_{\mathrm{v},f_{ij}})_{ii}$, is derived as follows:

$$(\widehat{F}_{\mathrm{v},f_{ij}})_{ii} = \frac{M_\infty}{Re_\infty}\frac{1}{2}\left\{\frac{\mu_i+\mu_j}{(\rho k)_i}+\sigma_k\left[\left(\frac{1}{\omega}\right)_i+\frac{\left(\frac{\rho k}{\omega}\right)_j}{(\rho k)_i}\right]\right\}\frac{k_j-k_i}{x_j-x_i} \tag{A.4}$$

Similarly, the off diagonal part, $(\widehat{F}_{\mathrm{v},f_{ij}})_{ij}$, is given as

$$\left(\widehat{F}_{\mathrm{v},f_{ij}}\right)_{ij} = \frac{M_\infty}{Re_\infty}\frac{1}{2}\left\{\frac{\mu_i+\mu_j}{(\rho k)_j}+\sigma_k\left[\frac{\left(\frac{\rho k}{\omega}\right)_i}{(\rho k)_j}+\left(\frac{1}{\omega}\right)_j\right]\right\}\frac{k_j-k_i}{x_j-x_i} \tag{A.5}$$

The additional contribution of the implicit operator, $\frac{\widehat{\partial F}_{\mathrm{v}}}{\partial(\rho k)}(\rho k)$, to the diagonal is given by

$$\left(\frac{\widehat{\partial F}_{\mathrm{v},f_{ij}}}{\partial(\rho k)}(\rho k)\right)_{ii} = \frac{M_\infty}{Re_\infty}\frac{1}{2}\left\{\left[-\frac{\mu_i+\mu_j}{(\rho k)_i}-\sigma_k\frac{\left(\frac{\rho k}{\omega}\right)_j}{(\rho k)_i}\right]\frac{k_j-k_i}{x_j-x_i}-\left\{\mu_i+\mu_j+\sigma_k\left[\left(\frac{\rho k}{\omega}\right)_i+\left(\frac{\rho k}{\omega}\right)_j\right]\right\}\frac{1}{\rho_i(x_j-x_i)}\right\} \tag{A.6}$$

In the present work, the evaluation of the convection flux term is based on the HLLC Riemann solver. Although the implementation of the implicit operator of the convection term corresponds to the HLLC solver, its application to other solvers is straightforward. The one-dimensional HLLC solver of the turbulent kinetic energy in Cartesian coordinates is defined by

$$F_{\mathrm{c},f_{ij}} = \begin{cases}(\rho u k)_i & S_i > 0\\ (\rho^* S_M k)_i & S_i \leqslant 0 < S_M\\ (\rho^* S_M k)_j & S_M \leqslant 0 \leqslant S_j\\ (\rho u k)_j & S_j < 0\end{cases} \tag{A.7}$$

where $(\rho^*)_i = [\rho(S-u)]_i$ (for specific definitions of the signal velocities S_i, S_j and S_M see the paper by Batten et al. [2]). The diagonal implicit operators, namely, $(\widehat{F}_{\mathrm{c},f_{ij}})_{ii}$ and $(\frac{\widehat{\partial F}_{\mathrm{c},f_{ij}}}{\partial(\rho k)}(\rho k))_{ii}$, are calculated as follows:

$$(\widehat{F}_{\mathrm{c},f_{ij}})_{ii} = \begin{cases}u_i & S_i > 0\\ (S_i-u_i)S_M & S_i \leqslant 0 < S_M\\ \frac{(\rho^* S_M k)_j}{(\rho k)_i} & S_M \leqslant 0 \leqslant S_j\\ \frac{(\rho u k)_j}{(\rho k)_i} & S_j < 0\end{cases} \tag{A.8}$$

$$\left(\frac{\widehat{\partial F}_{\mathrm{c},f_{ij}}}{\partial(\rho k)}(\rho k)\right)_{ii} = \begin{cases}0 & S_i > 0\\ 0 & S_i \leqslant 0 < S_M\\ -\frac{(\rho^* S_M k)_j}{(\rho k)_i} & S_M \leqslant 0 \leqslant S_j\\ -\frac{(\rho u k)_j}{(\rho k)_i} & S_j < 0\end{cases} \tag{A.9}$$

The off-diagonal Jacobian of the convection flux is obtained in similar fashion to the diffusion implicit operator.

Finally, the source term of the TNT turbulence model is defined as

$$S^{\mathrm{t}} = \begin{Bmatrix} P_k - \beta^*\rho k\omega\frac{Re_\infty}{M_\infty} \\ \alpha\frac{\omega}{k}P_k - \beta\rho\omega^2\frac{Re_\infty}{M_\infty} + C_{\mathrm{D}}\end{Bmatrix} \tag{A.10}$$

For the sake of simplicity, the cross-diffusion term, $C_{\mathrm{D}} = \sigma_d\frac{\rho}{\omega}\mathrm{Max}[\frac{\partial k}{\partial x_j}\frac{\partial\omega}{\partial x_j},0]\frac{M_\infty}{Re_\infty}$, is treated as a constant.

According to steps 1 and 2, the source term may be rewritten as follows:

$$S^{t}=\begin{Bmatrix} \mu_{t}\left[\left(\frac{\partial u_i}{\partial x_j}+\frac{\partial u_j}{\partial x_i}\right)-\frac{2}{3}\delta_{ij}\frac{\partial u_k}{\partial x_k}\right]\frac{\partial u_i}{\partial x_j}\frac{M_\infty}{Re_\infty}-\frac{2}{3}\rho k\delta_{ij}\frac{\partial u_i}{\partial x_j}-\beta^{*}\frac{(\rho k)^2}{\mu_t}\frac{Re_\infty}{M_\infty} \\ \alpha\rho\left[\left(\frac{\partial u_i}{\partial x_j}+\frac{\partial u_j}{\partial x_i}\right)-\frac{2}{3}\delta_{ij}\frac{\partial u_k}{\partial x_k}\right]\frac{\partial u_i}{\partial x_j}\frac{M_\infty}{Re_\infty}-\frac{2}{3}\alpha\rho\omega\delta_{ij}\frac{\partial u_i}{\partial x_j}-\beta\rho\omega^2\frac{Re_\infty}{M_\infty}+C_{D} \end{Bmatrix} \tag{A.11}$$

In practice, step 2 is skipped since k does not appear in the turbulence specific dissipation rate equation.

Following step 3, the source term becomes

$$S^{t}=\begin{Bmatrix} \frac{\rho k}{\omega}\left[\left(\frac{\partial u_i}{\partial x_j}+\frac{\partial u_j}{\partial x_i}\right)-\frac{2}{3}\delta_{ij}\frac{\partial u_k}{\partial x_k}\right]\frac{\partial u_i}{\partial x_j}\frac{M_\infty}{Re_\infty}-\frac{2}{3}\rho k\delta_{ij}\frac{\partial u_i}{\partial x_j}-\beta^{*}\frac{(\rho k)^2}{\mu_t}\frac{Re_\infty}{M_\infty} \\ \alpha\rho\left[\left(\frac{\partial u_i}{\partial x_j}+\frac{\partial u_j}{\partial x_i}\right)-\frac{2}{3}\delta_{ij}\frac{\partial u_k}{\partial x_k}\right]\frac{\partial u_i}{\partial x_j}\frac{M_\infty}{Re_\infty}-\frac{2}{3}\alpha\rho\omega\delta_{ij}\frac{\partial u_i}{\partial x_j}-\beta\rho\omega^2\frac{Re_\infty}{M_\infty}+C_{D} \end{Bmatrix} \tag{A.12}$$

Then the diagonal term of the first part of the source term Jacobian, namely, $[\widehat{S}^{t}]$, takes the form

$$[\widehat{S}^{t}]=[I]\begin{Bmatrix} \frac{1}{\omega}\left[\left(\frac{\partial u_i}{\partial x_j}+\frac{\partial u_j}{\partial x_i}\right)-\frac{2}{3}\delta_{ij}\frac{\partial u_k}{\partial x_k}\right]\frac{\partial u_i}{\partial x_j}\frac{M_\infty}{Re_\infty}-\frac{2}{3}\delta_{ij}\frac{\partial u_i}{\partial x_j}-\beta^{*}\frac{\rho k}{\mu_t}\frac{Re_\infty}{M_\infty} \\ \frac{\alpha}{\omega}\left[\left(\frac{\partial u_i}{\partial x_j}+\frac{\partial u_j}{\partial x_i}\right)-\frac{2}{3}\delta_{ij}\frac{\partial u_k}{\partial x_k}\right]\frac{\partial u_i}{\partial x_j}\frac{M_\infty}{Re_\infty}-\frac{2}{3}\alpha\delta_{ij}\frac{\partial u_i}{\partial x_j}-\beta\omega\frac{Re_\infty}{M_\infty}+\frac{C_{D}}{\rho\omega} \end{Bmatrix} \tag{A.13}$$

and the second part of the Jacobian, namely, $[\widehat{\frac{\partial S^{t}}{\partial U^{t}}}U^{t}]$ is given by

$$\left[\frac{\partial\widehat{S}^{t}}{\partial U^{t}}U^{t}\right]=[I]\begin{Bmatrix} -\beta^{*}\frac{\rho k}{\mu_t}\frac{Re_\infty}{M_\infty} \\ -\frac{\alpha}{\omega}\left[\left(\frac{\partial u_i}{\partial x_j}+\frac{\partial u_j}{\partial x_i}\right)-\frac{2}{3}\delta_{ij}\frac{\partial u_k}{\partial x_k}\right]\frac{\partial u_i}{\partial x_j}\frac{M_\infty}{Re_\infty}-\beta\omega\frac{Re_\infty}{M_\infty}-\frac{C_{D}}{\rho\omega} \end{Bmatrix} \tag{A.14}$$

References

[1] G. Barakos, D. Drikakis, Implicit unfactored implementation of two-equation turbulence models in compressible Navier–Stokes methods, International Journal For Numerical Methods In Fluids 28 (1) (1998).

[2] P. Batten, M.A. Leschziner, U.C. Goldberg, Average-state Jacobians and implicit methods for compressible viscous and turbulent flows, Journal of Computational Physics 137 (1) (1997).

[3] A. Berman, R.J. Plemmons, Nonnegative Matrices in the Mathematical Sciences, Computer Science and Applied Mathematics, Academic Press Inc., London, 1979, ISBN 0-12-092250-9.

[4] P. Catalano, M. Amato, An evaluation of RANS turbulence modeling for aerodynamic applications, Aerospace Science and Technology 7 (2003).

[5] R.F. Chen, Z.J. Wang, Fast, block lower-upper symmetric Gauss–Seidel scheme for arbitrary grids, AIAA Journal 38 (12) (2000).

[6] D. Coles, A.J. Wadcock, Flying-hot-wire study of flow past an NACA4412 airfoil at maximum lift, AIAA Journal 17 (4) (1979).

[7] P.H. Cook, M.A. McDonald, M.C.P. Firmin, Aerofoil RAE2822-pressure distributions, boundary layer and wake measurements, AGARD-AR-138, 1979.

[8] T. Du, Z.-N. Wu, Mixed analytical/numerical method for low-Reynolds-number k–ϵ turbulence models, AIAA Journal 42 (6) (2004).

[9] T. Du, Z.-N. Wu, Mixed analytical/numerical method applied to the high Reynolds number k–ϵ turbulence model, Computers & Fluids 34 (1) (2005).

[10] W. Haase, F. Bradsma, E. Elsholz, M.D.S. Leschziner, EUROVAL – An European Initiative on Validation of CFD Codes. vol. 42, 1992.

[11] P.G. Huang, T.J. Coakley, An implicit Navier–Stokes code for turbulent flow modeling. In: 30th AIAA Aerospace Sciences Meeting and Exhibit. Reno, NV, AIAA paper 92-0547, January 1992.

[12] F. Ilinca, D. Pelletier, Positivity preservation and adaptive solution for the k–ϵ model of turbulence, AIAA Journal 36 (1) (1998).

[13] F. Ilinca, D. Pelletier, Positivity preservation and adaptive solution of two-equation models of turbulence, International Journal of Thermal Sciences 38 (7) (1999).

[14] A. Jameson, S. Yoon, Lower-upper implicit schemes with multiple grids for the Euler equations, AIAA Journal 25 (7) (1987).

[15] P. Jawahar, H. Kamath, A high-resolution procedure for Euler and Navier–Stokes computations on unstructured grids, Journal of Computational Physics 164 (1) (2000).

[16] J.C. Kok, Resolving the dependence on freestream values for the k–ω turbulence model, AIAA Journal 38 (7) (2000).

[17] P.J. Lamont, The complex asymmetric flow over a 3.5D ogive nose and cylindrical afterbody at high angles of attack. In: 20th AIAA Aerospace Sciences Meeting, Orlando, FL, AIAA Paper 82-0053, January 1982.

[18] B.E. Launder, B.I. Sharma, Application of the energy-dissipation model of turbulence to the calculation of flow near a spinning disc, Letters in Heat and Mass Transfer 1 (2) (1974).

[19] F.-S. Lien, G. Kalitzin, Computations of transonic flow with the $v^2 - f$ turbulence model, International Journal of Heat and Fluid Flow 22 (1) (2001).
[20] F. Liu, X. Zheng, A strongly coupled time-marching method for solving the Navier–Stokes and k–ω turbulence model equations with multigrid, Journal of Computational Physics 128 (2) (1996).
[21] H. Luo, J.D. Baum, R. Lohner, Computation of compressible flows using a two-equation turbulence model on unstructured grids, International Journal of Computational Fluid Dynamics 17 (1) (2003).
[22] D.J. Mavriplis, L. Martinelli, Multigrid solution of compressible turbulent flow on unstructured meshes using a two-equation model, International Journal for Numerical Method in Fluids 18 (1994).
[23] F.R. Menter, Zonal two equation k–ω turbulence models for aerodynamic flows. In: 24th AIAA Fluid Dynamics Conference. Orlando, FL, AIAA paper 93-2906, July 1993.
[24] B. Merci, J. Steelant, J. Vierendeels, K. Riemslagh, E. Dick, Computational treatment of source terms in two-equation turbulence models, AIAA Journal 38 (11) (2000).
[25] C.L. Merkle, M. Deshpande, S. Venkateswaran, Efficient implementation of turbulence modeling in computational schemes, in: Proceedings of the Second US National Congress on Computational Mechanics, Pergamon, Oxford, 1993.
[26] P.R. Spalart, S.R. Allmaras, A one-equation turbulence model for aerodynamic flows. AIAA paper 92-0439, 1992.
[27] V. Venkatakrishnan, Convergence to steady state solutions of the Euler equations on unstructured grids with limiters, Journal of Computational Physics 118 (1) (1995).
[28] D.C. Wilcox, Reassessment of the scale-determining equation for advanced turbulence models, AIAA Journal 26 (11) (1988).
[29] D.C. Wilcox, Comparison of two-equation turbulence models for boundary layers with pressure gradient, AIAA Journal 31 (8) (1993).
[30] D.C. Wilcox, Turbulence Modeling for CFD, Second ed., CDW Industries Inc., La Canada, California, 1998, ISBN 1-928729-10-X.
[31] Z. Yang, T.H. Shih, New time scale based k–ϵ model for near-wall turbulence, AIAA Journal 31 (7) (1993).